Fabrication of antibacterial polydopamine-carboxymethyl cellulose-Ag nanoparticle hydrogel coating for urinary catheters

Cai, Yongwei; Gu, Ronghua; Dong, Yuhang; Zhao, Qi; Zhang, Ke; Cheng, Changyuan

Published in:
Journal of Biomaterials Applications

DOI:
10.1177/08853282231173576

Publication date:
2023

Document Version
Peer reviewed version

Cai, Y, Gu, R, Dong, Y, Zhao, Q, Zhang, K, Cheng, C, Yang, H, Li, J & Yuan, X 2023, 'Fabrication of antibacterial polydopamine-carboxymethyl cellulose-Ag nanoparticle hydrogel coating for urinary catheters', Journal of Biomaterials Applications, vol. 38, no. 1, pp. 73 - 84. https://doi.org/10.1177/08853282231173576

Fabrication of antibacterial polydopamine-carboxymethyl cellulose-Ag nanoparticle hydrogel coating for urinary catheters

Yongwei Cai [1,*], Ronghua Gu [2], Yuhang Dong [3], Qi Zhao [3,*], Ke Zhang [3], Changyuan Cheng [3], Hong Yang [1], Jianxiang Li [1], Xing'gen Yuan [1]

[1] *School of Chemistry and Chemical Engineering, Chongqing University of Technology, Chongqing 400054, China*

[2] *Chongqing University Cancer Hospital, Chongqing 400030, China*

[3] *School of Science and Engineering, University of Dundee, Dundee DD1 4HN, UK*

Corresponding authors:

Yongwei Cai – Email: cyw@cqut.edu.cn; Qi Zhao – Email: q.zhao@dundee.ac.uk.

ABSTRACT

Urinary tract infections caused by catheter insertion are prevalent in hospital clinics, which can induce serious complications such as bacteriuria and sepsis, and even lead to patient death. The disposable catheters currently used in clinical practice suffer from poor biocompatibility and high infection rate. In this paper, we developed a polydopamine (PDA)-carboxymethylcellulose (CMC)-Ag nanoparticles (AgNPs) coating with both good antibacterial and anti-adhesion properties to bacteria on the surfaces of a disposable medical latex catheter by a simple dipping method. The antibacterial efficiency of the coated catheters against Gram-negative *E. coli* and Gram-positive *S. aureus* bacteria

was evaluated with both inhibition zone tests and fluorescence microscopy. Compared with the untreated catheter, the PDA-CMC-AgNPs coated catheters showed both good antibacterial and anti-adhesion properties to bacteria, which inhibited the adhesion of live bacteria and dead bacteria by 99.0% and 86.6%, respectively. This novel PDA-CMC-AgNPs composite hydrogel coating has great potential in applications in catheters and other biomedical devices to reduce infections.

Keywords: Urinary catheter; polydopamine; Ag nanoparticles; carboxymethylcellulose; antibacterial hydrogel.

Introduction

Catheter-associated Urinary Tract Infections (CAUTIs) are prevalent in hospital clinical and healthcare settings and can induce serious complications such as bacteriuria, sepsis, and even lead to patient death [1]. Disposable urinary catheters are likely contaminated with bacterial colonies within hours of placement [2, 3], eventually forming a biofilm [4]. This biofilm is extremely difficult to be removed and is highly resistant to most antibiotics [5]. According to statistics, the world average infection rate for CAUTIs caused by catheter insertion is 33%, accounting for 40% of hospital-acquired infections [6]. Currently, the catheters used in hospital clinics are mainly made of silicone, latex, and polyvinyl chloride (PVC), which do not have any antiseptic properties [7, 8]. Due to the occurrence of CAUTIs on the disposable catheters, it is clinically necessary to change catheters several times to prevent CAUTIs, which increases the psychological stress, discomfort or pain of patients [9]. It not only prolongs patients' hospital stays and increases their financial burden, but also causes a huge waste of medical resources. Therefore, tremendous efforts have been made to modify

the surface of the disposable urinary catheters to prevent the growth of biofilm and hence to reduce the occurrence of CAUTIs [7].

The antibacterial catheters currently used in clinical practice are mainly based on two preparation techniques [10]. One is adding antibacterial drugs on the catheter surface before leaving the factory or before clinical application. However, this method has the drawbacks of being cumbersome to use, such as the susceptibility to secondary contamination, high requirements for drug addition and encapsulation during production, cumbersome production processes, and the susceptibility of bacteria to develop drug resistance [11]. Another technique is to coat heavy metals with antibacterial properties on the catheter surfaces. The commonly used antibacterial heavy metals include Ag nanoparticles (AgNPs) [12-14], nano-Au [15] and Cu^{2+} [16] etc. Among them, Ag has the strongest antibacterial ability and the smallest minimum inhibitory concentration (MIC) and is not easy to develop drug resistance [17, 18]. However, direct vapor deposition of Ag coating on the catheter surface suffers from the problem of oxidation, leading to poor antibacterial efficiency or even peeling off from the catheter surface [19].

Inspired by the ability of marine mussels to adhere firmly to the object surfaces such as reefs and ship bottoms, Haeshin Lee et al. [20] in 2007 prepared polydopamine (PDA) by self-polymerization *via* Schiff-base type reactions (with amine containing molecules) or Michael type reactions (with amine and thiol-containing molecules) at mildly basic pH on various substrates (metals and oxides, ceramics, semiconductors and polymers, etc.). They found that PDA has strong adhesion properties and can act as a versatile mediate binding to graft polymer coatings. [20]

Furthermore, PDA is a component of natural melanin and therefore possesses excellent optical, electrical and biocompatibility properties.[21] As a result, PDA nowadays has attracted considerable interest for various types of applications, such as biomaterials [22], implant surface modification [21], drug delivery [23, 24], proteins immobilization [25], nanocapsules [26, 27], nanoparticles stabilization [28], fouling-resistant layer on water purification membranes [29]. For example, Huang et al. [30] immobilized bioactive carboxymethyl chitosan (CMCS) on cathodic plasma electrolytic deposition (CPED)-treated Mg alloy substrate with a PDA intermediate layer. The result indicates that PDA promotes the adhesion to the substrate. Xu et al. [31] designed a PDA coating with AgNPs on TiO_2 nanotube arrays. The PDA layer was employed as both reductant and adhesive agent to reduce Ag^+ to AgNPs and strengthen the adhesion between AgNPs and the TiO_2 nanotube surface.

Furthermore, PDA does not induce cytotoxicity as intermediate layer and exhibited excellent biocompatibility. For instance, Lee et al. [20] prepared PDA-coated methoxy-poly(ethylene glycol) [(mPEG-NH_2 or mPEG-SH) surfaces on glasses, which exhibit substantial reduction in nonspecific protein adsorption and dramatic reduction of fibroblast cell attachment. Ku et al. [32] reported that PDA has no adverse effects on the proliferation or viability of various mammalian cells, including osteoblasts, endothelial cells, neurons and fibroblasts. Liu et al. [33] found that that polydopamine nanoparticles did not induce obvious cytotoxic effects when in contact with both the mouse 4T1 breast cancer cells and the human cervical cancer cells (HeLa cells), even at very high doses. Zhong et al. [34] modified titanium dioxide nanotubes with PDA and found that PDA modification promotes endothelial cell (EC) attachment, proliferation, migration, and release of nitric oxide.

On the other hand, hydrogels have three-dimensional polymeric network structures [35] and have been extensively applied as effective protecting layers for reducing bacteria adhesion [36-40], due to their excellent biocompatibility [41], functional group density [42], super-lubricity [43], and super-stretchability [44]. Therefore, coating hydrogels onto urinary catheter surfaces with super-slip properties significantly improves the smoothness and lubricity of the catheter which can minimize the difficulty of catheter insertion [8]. Common hydrogels such as sodium carboxymethylcellulose(CMC) hydrogel structures have excellent swell-ability and viscodynamic elasticity, and strong complexation to many metal ions [45, 46]. As a result, the combination of inorganic Ag nanoparticles and CMC hydrogel networks would generate new composite coating materials [47] for the urinary catheters.

Considering the mentioned matters, in the present research, we intended to develop a novel polydopamine-carboxymethylcellulose-Ag nanoparticles (PDA-CMC-AgNPs) composite coating on the surface of the disposable catheters based on high adhesion between PDA and catheter substrates, as well as the powerful complexing effect between CMC and AgNPs. First, we modified the catheter with PDA to act as an interlayer to bind the CMC hydrogel coating and the catheter substrate. Then we prepared the AgNPs colloid and the CMC-AgNPs hydrosol, and then coated the hydrosol on the urinary catheter surface with simple dipping method. Whereafter, we characterized the as-prepared coated urinary catheters by FESEM, EDS and XPS analysis. We also studied the liquid contact angles and surface energy of the samples. Finally, we evaluated the antibacterial effect of the coated catheters with Gram-negative *E. coli* and Gram-positive *S. aureus* bacteria.

Experimental section

Reagents and materials

Dopamine hydrochloride (98 %, Mw =600 Da), tris-hydroxymethylaminomethane hydrochloride (Tris-HCl), sodium carboxymethylcellulose (CMC, average Mw ~90,000), polyvinyl pyrrolidone (PVP), anhydrous ethanol, succinic acid (SA), silver nitrate, ciprofloxacin (CPFX), acetic acid, glucose (Glu), trisodium citrate (TC), benzophenone, and UV initiator Irgacure 2959 were purchased from Sigma-Aldrich (U.K.). Diiodomethane and formamide were supplied by Sichuan Chengdu Kolon Chemical Co., Ltd., China. All these chemicals and reagents were used without further purification. Gram-negative *Escherichia coli* (*E. coli*, WT F1693) and Gram-positive *Staphylococcus aureus* (*S. aureus*, F1557) were purchased from the Institute of Infection and Immunity, University of Nottingham, U. K. The disposable sterile Foley type double-lumen medical latex urinary catheters (STAR-14Fr) were purchased from Zhanjiang Shida Industrial Co., China. All the solvents and reagents were analytical grade.

Preparation of PDA-CMC-AgNPs composite coatings

Scheme 1 presents the preparation process of the PDA-CMC-AgNPs coating on the catheter segment. The brief preparation scheme of PDA-CMC-AgNPs composite coating on the latex urinary catheters includes three steps.

Step 1: Modifying the catheter with PDA intermediate layer

The standard sterile latex urinary catheter was cut into 1.2 ± 0.1 cm long segments and then cleaned ultrasonically with anhydrous ethanol and deionized water, respectively, and then activated by ethanol solution of 10% benzophenone and dried for use. The PDA coating worked as an intermediate layer was prepared by impregnating the activated catheter segments in dopamine hydrochloride (DPA) /Tris-HCl (pH=8.5) solution at 50 ℃, kept in dark for 10 h [20].

Stept 2: Preparing the AgNPs colloid

$AgNO_3$ solution with different concentrations (0.01-0.05 M) was boiled and kept in dark place under magnetic stirring. Appropriate amount of 1 *wt*. % sodium citrate aqueous solution and glucose as reducing agents were slowly added into the $AgNO_3$ solution to change the solution from colorless to light yellow or light brown to prepare AgNPs colloidal solution [48, 49], and then cooled to room temperature for further use.

Stept 3: Preparing PDA-CMC-AgNPs composite coatings

Firstly, the appropriate amount of CMC powder was completely dissolved in the prepared AgNPs colloidal solution under magnetic stirring. Succinic acid (SA) as the cross-linking agent, PVP as the anti-swelling reagent, and Irgacure 2959 as the UV initiator were added to the CMC pregel solution, separately [50], and the CMC-AgNPs pre-sol was finally prepared. To compare the CMC-AgNPs coatings with antibacterial properties, a certain amount of antibacterial agent, ciprofloxacin (CPFX), was pre-dissolved in acetic acid aqueous solution and then added to the CMC-AgNPs pregel. Secondly, the activated catheter segment was then dip-coated in the pregel solution for 2-10 min at room temperature, followed by an ultraviolet light treatment with a specific

light wavelength of 365 nm for 30 min to stimulate the polymerization and the cross-linking reaction of the coating. The catheter was rotated at 20 s/circle during the curing reaction to ensure full exposure to the UV light. Finally, the prepared coating samples were rinsed with ethanol and deionized water, respectively, and then dried at room temperature.

The whole unitary catheter was also coated under the optimized coating conditions to obtain a dense and uniform coating. For comparison, the PDA, the PDA-CMC-AgNPs, and the CMC-AgNPs coatings were also prepared by changing the above coating preparation steps. Moreover, the coatings on the stainless steel (SS) substrates were also prepared by the same method.

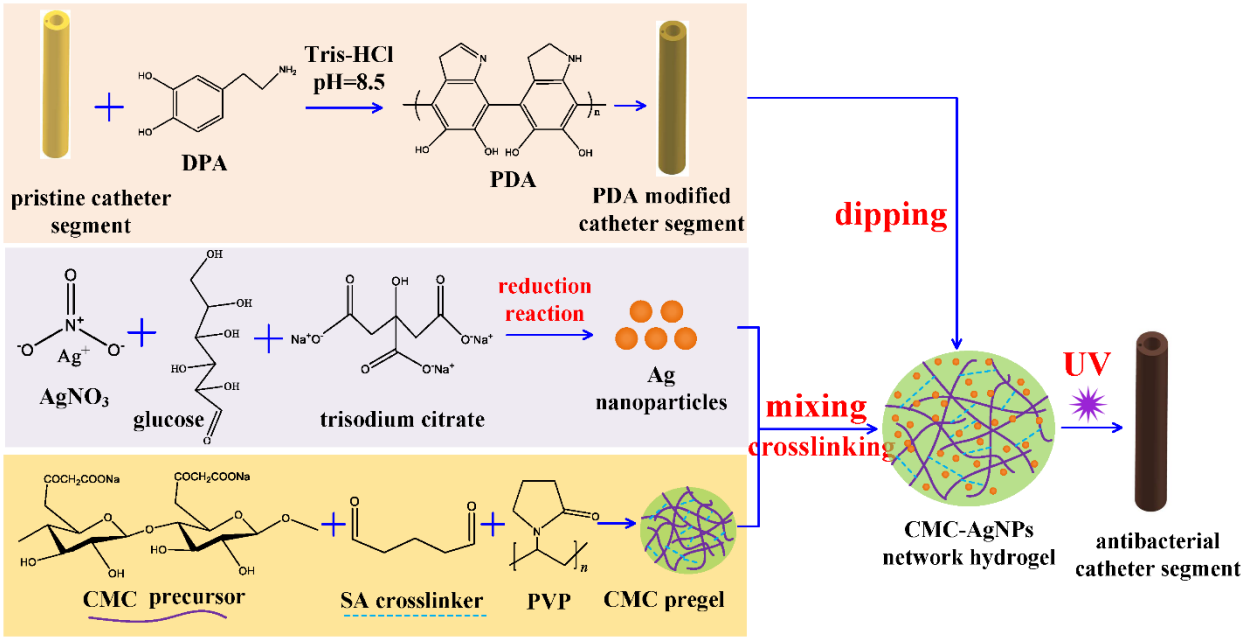

Scheme 1 Schematic diagram for the preparation of antibacterial PDA-CMC-AgNPs coating on urinary catheter segments.

Characterisation and measurement

TEM

Transmission electron microscopy (TEM) analysis was performed with a JEM-1230 (JEOL,Tokyo, Japan) at an accelerating voltage of 100 kV to characterize the particle size of the AgNPs in the AgNPs colloidal solution. The mean value as well as the corresponding standard deviation of the particle size was determined with no less than 10 AgNPs.

AFM

The surface topography and the surface roughness of the samples were detected by AFM using a Nanoscope V Multimode 8 scanning probe microscope from Bruker Corporation. The roughness analysis option was applied to perform roughness analyses on 5.0 μm × 5.0 μm and 20.0 μm × 20.0 μm imaged surface areas for each sample. Results are presented as *R*a (arithmetic average roughness) and *R*q (root mean square deviation) values [51]. All experiments were carried out with the same AFM probe under ambient conditions (temperature of 25ºC, relative humidity of 25%).

FE-SEM

Surface morphologies of the samples were characterized by Zeiss FESEM (Carl Zeiss, Model Neon 40 EsB CrossBeam, Germany) at a voltage of 2 kV. Chemical compositions were explored using EDS (Energy Dispersive Spectrometer).

XPS

The chemical composition of the coating on the siliconized latex catheter was characterized using an X-ray photoelectron spectroscopy (XPS, Thermo Scientific Escalab 250Xi, USA) with Al

radiation under the scan resolution of 0.1 eV, the scan voltage of 15 kV, and the electric current of 12.8 mA. CasaXPS software (Casa Software Ltd.; http://www.casaxps.com/) was used to analyze and process the XPS data and individual peaks were fitted to a Gaussian/Lorentzian (GL) function for each component of the element envelopes.

Wettability and Surface Free Energy

The wettability of the sample surfaces was tested using a video optical contact angle meter (DropMeterTM A-200, MAIST Vision Inspection & Measurement Co., China). The surface free energy was also calculated using the system of equations method (Das) [52]. That is, three standard liquids, water (W), formamide (FMD), and diiodomethane (DIM), were selected to measure the contact angles of the samples, and the individual surface energy components (γ_l^{LW}, γ_l^{+}, and γ_l^{-}) of the standard liquids were obtained from the literature [52]. These surface energy components were then substituted into the Van Oss equations (1)-(3) to obtain the individual surface energy components (γ_s^{LW}, γ_s^{+} and γ_s^{-}) of the sample surface. Finally, the total surface energy, γ_s, of the solid could be calculated by substituting equation (4). [52]

$$\gamma_{l,W}(1+\cos\theta_W) = 2\left(\sqrt{\gamma_{l,W}^{LW}\cdot\gamma_S^{LW}} + \sqrt{\gamma_{l,W}^{+}\cdot\gamma_s^{-}} + \sqrt{\gamma_{l,W}^{-}\cdot\gamma_S^{+}}\right) \quad (1)$$

$$\gamma_{l,FMD}(1+\cos\theta_{FMD}) = 2\left(\sqrt{\gamma_{l,FMD}^{LW}\cdot\gamma_S^{LW}} + \sqrt{\gamma_{l,FMD}^{+}\cdot\gamma_s^{-}} + \sqrt{\gamma_{l,FMD}^{-}\cdot\gamma_S^{+}}\right) \quad (2)$$

$$\gamma_{l,DIM}(1+\cos\theta_{DIM}) = 2\left(\sqrt{\gamma_{l.DIM}^{LW}\cdot\gamma_S^{LW}} + \sqrt{\gamma_{l,DMI}^{+}\cdot\gamma_s^{-}} + \sqrt{\gamma_{l,DMI}^{-}\cdot\gamma_S^{+}}\right) \quad (3)$$

$$\gamma_S = \gamma_S^{LW} + 2\sqrt{\gamma_S^{+}\cdot\gamma_S^{-}} \quad (4)$$

Antibacterial performance assay

Inhibition zone test

Gram-negative bacteria *Escherichia coli* (*E. coli*, WT F1693) and gram-positive bacteria *Staphylococcus aureus* (*S. aureus*, F1557) were selected for the study, and the samples were tested for their antibacterial activity using inhibition zone test [53]. The bacterial concentrations were adjusted to 10^7 colony-forming units (CFUs)·mL^{-1} in the antibacterial assay and dispersed uniformly on the surface of Luria-Bertani Agar plate. The catheter segment was inserted vertically into the hole of the agar plate. The hole in the agar plate was made with a sterilized stainless steel punch, and the outer diameter of the punch was the same as the outer diameter of the catheter. The antibacterial performance against *E. coli* was determined by using various coated urinary catheters and the untreated catheter as a control. The agar plate was incubated at 37°C for 24 h before measuring the diameter of the inhibition zone.

Live/dead Assay: Fluorescence Microscopy

To further evaluate the antibacterial property and anti-adhesion efficacy of the as-prepared coatings, the samples with adhered bacteria were stained using SYTO™9/PI (propidium iodide) and propidium iodide (PI) and then were observed using an Olympus Fluorescence Microscope (BX41, Tokyo, Japan) with live bacteria appearing green and dead bacteria appearing red under fluorescence irradiation. Quantitative analysis was performed by the image analysis software Image-ProPlus® by counting the numbers of the dead and live bacteria based on the fluorescence intensity of the images

[14]. All green fluorescence was found under fluorescence microscope when the silicone catheter was used for observation, because the silicone catheter underwent fluorescence reaction under fluorescence irradiation. Therefore, the microscope was unable to observe and identify the number of live bacteria. Consequently, a stainless steel (SS) sheet (25 ×25 ×1 mm) was selected as the substrate and the coatings were prepared under the identical conditions as the urinary catheter did. All samples were observed after 2 h of impregnation with Gram-positive *S. aureus* solution.

The above experiments were repeated three times independently. All statistical analyses were carried out using analysis of ANOVA testing within Microsoft Excel (Microsoft Corp., Redmond, USA). Values are reported in the paper as mean values with standard deviations.

Results and discussion

Preparation of PDA-CMC-AgNPs hydrogel coating on urinary catheter

Figure 1a shows that the nano-Ag colloid solution after reduction of 0.01 M $AgNO_3$ solution by trisodium citrate and glucose, had obvious nano-Ag colloid light path after laser irradiation. Figure 1b reveals the well-dispersed quasi-spherical-shaped AgNPs [54] with the average diameter of 24.5 ± 4.1 nm and a relatively narrow particle size distribution (Figure 1c).

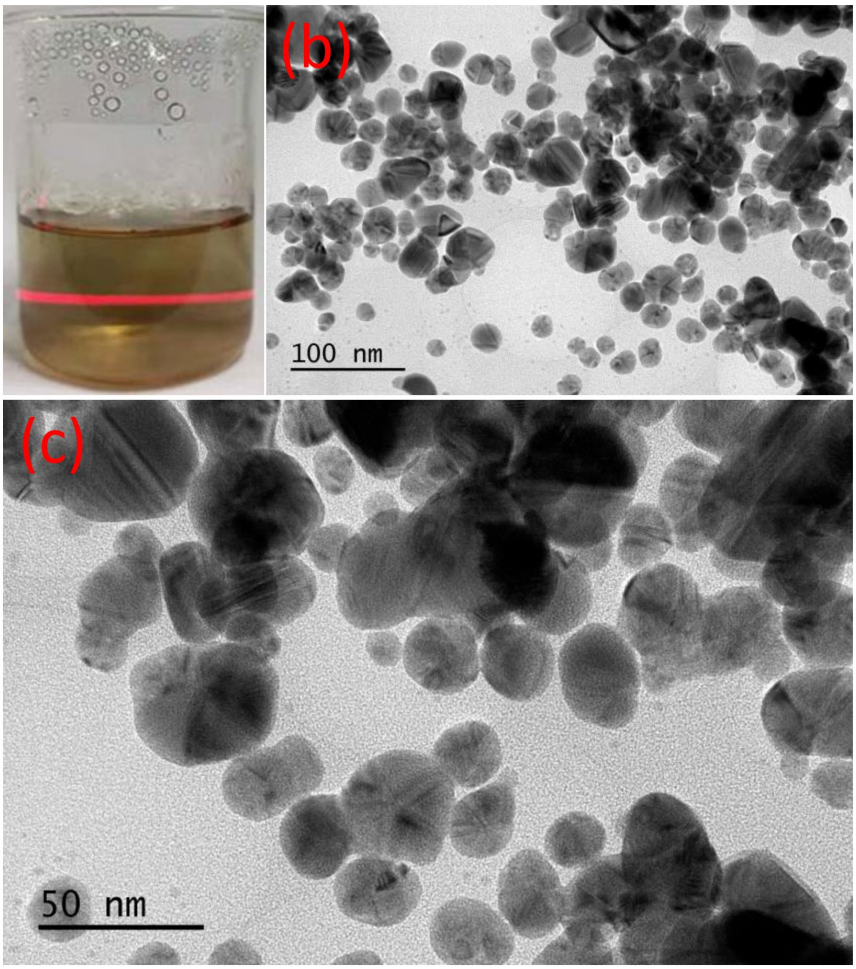

Figure 1 Photograph of the nano-Ag colloid solution prepared with 0.01 M $AgNO_3$ solution and TEM micrographs of Ag nanoparticles. (a): the nano-Ag colloid solution with obvious colloid light path after laser irradiation; (b) and (c): The TEM microstructure of the Ag colloid with lower and higher magnifications, respectively.

Figure S1a shows that the polydopamine solution had brownish-black color with suspended polydopamine particles. Figure S1b displays the hydrogel solution formed by dissolving sodium carboxymethyl cellulose into the nano-Ag colloid solution, which also had obvious nano-Ag colloidal laser light paths. Figure S1c illustrates the photographs of the urinary catheter segments

with the PDA or the PDA-CMC-Ag coating. Figure S1d exhibits the photographs of the whole urinary catheter, in which the top one was the original urinary catheter, the middle one was the urinary catheter with the PDA coating, and the bottom one was the urinary catheter coated with the PDA-CMC-Ag nanoparticles. Figure S1e shows the photographs of the prepared coated urinary catheter segments before and after rubbing with an A_4 paper, respectively. Although the coated urinary catheter became darker after rubbing violently, no obvious coating abrasion marks were found on the coated catheter surface. Furthermore, when the coated catheter was bent by hand and then wiped lightly with a wet paper towel, no coating material was peeled off from the urinary catheter surface, indicating that the bond strength between the coating and the urinary catheter surface was very strong. Figure S1f shows the photograph of the uncoated Foley-type urinary catheter segment, which is composed of the siliconized layer and the latex body.

Surface morphology and chemical characterisation

AFM

Figure 2 presents typical surface topography images of the original catheter and the PDA-CMC-AgNPs (0.01 M) coating prepared on the catheter with three-dimensional AFM measurements in scan areas of 5.0 μm × 5.0 μm and 20.0 μm × 20.0 μm for each sample. The original catheter consisted of many particle peaks and valleys, which distributed randomly on the surface (Figures 2a and 2b). The values of *R*a and *R*q were 48.0 nm and 65.8 nm in the scan area of 5.0 μm × 5.0 μm, respectively (Figure 2a). Compared with the original catheter, the values of *R*a and *R*q of the PDA-CMC-AgNPs (0.01 M) coating were 21.2 nm and 32.2 nm with the same size of the scan area (Figure

2c), respectively, which revealed a smoother surface. The results demonstrated that the obtained low roughness values of the hydrogel coating might contribute to the super-lubricity property of the coated catheter. It was also found that both the *R*a and *R*q values were increased sharply with the increase of the scan area for the same sample. For example, the *R*a and *R*q values of the original catheter surface increased to 243.0 nm and 307.0 nm, respectively, in the scan area of 20.0 μm × 20.0 μm. Similarly, the *R*a and *R*q values of the PDA-CMC-AgNPs (0.01 M) coating increased to 76.4 nm and 105.0 nm (Figure 2d), respectively, which were still significantly smaller than those of the original catheter with the same size of the scan area. The occurrence of increasing surface roughness with increasing scan area could be associated with the dependency of the roughness on the spatial wavelength of the scanned area or the frequency. [55] In particular, the *R*a and *R*q data of the PDA-CMC-AgNPs (0.01 M) coating significantly decreased in both AFM scan areas compared with those of the original catheter surface.

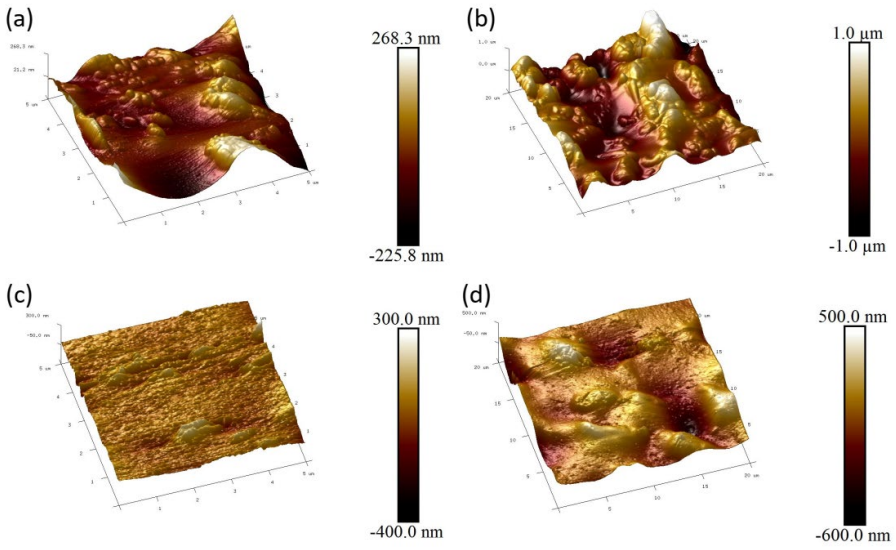

Figure 2 Three-dimensional AFM images of the samples. (a) and (b): the original catheter in a

scan area of 5.0 μm × 5.0 μm and 20.0 μm × 20.0 μm, respectively. (c) and (d): the PDA-CMC-AgNPs (0.01 M) coating prepared on the catheter in a scan area of 5.0 μm × 5.0 μm and 20.0 μm × 20.0 μm, respectively.

FE-SEM

Figures 3a-3c show the FE-SEM images of the original urinary catheter at different magnifications. The results indicated that the original catheter surface had a large number of irregular latex particle tissue with dense arrangement. Figures 3d-3f demonstrate the surface morphology of the PDA-CMC-AgNPs (0.01 M) coating at different magnifications. It was found that a thin film was formed on the catheter after coating PDA-CMC-AgNPs composites, and many irregular CMC tissue accumulations were found at high magnification, indicating that the coating was successfully attached to the urinary catheter surface (Figure 3e). Figure 3f presents that many spherical particles with a diameter of about 20 nm were accumulated on the CMC particle tissue, which were nano-Ag particles, as evidenced by EDS analysis (see Figure 3m). Figures 3g-3i show the microtopography of PDA coating on the 304 stainless steel (SS) substrate. Lots of dense PDA particles were accumulated on the 304 SS substrate, indicating that the PDA coating had successfully formed on the SS substrate.

Figures 3j and 3l show the block diagrams of EDS elemental tests in the analysis area corresponding to Figures 3a and 3d, respectively. The EDS analysis illustrates that the original catheter was mainly composed of C, O, and Si elements, which came from the siliconized latex urinary catheter (Figure 3k). In contrast, after coated with PDA, CMC and AgNPs composites, the

composition of the elements on the urinary catheter surfaces also included 2.70 *at*. % Ag content in the coating composition (Figure 3m).

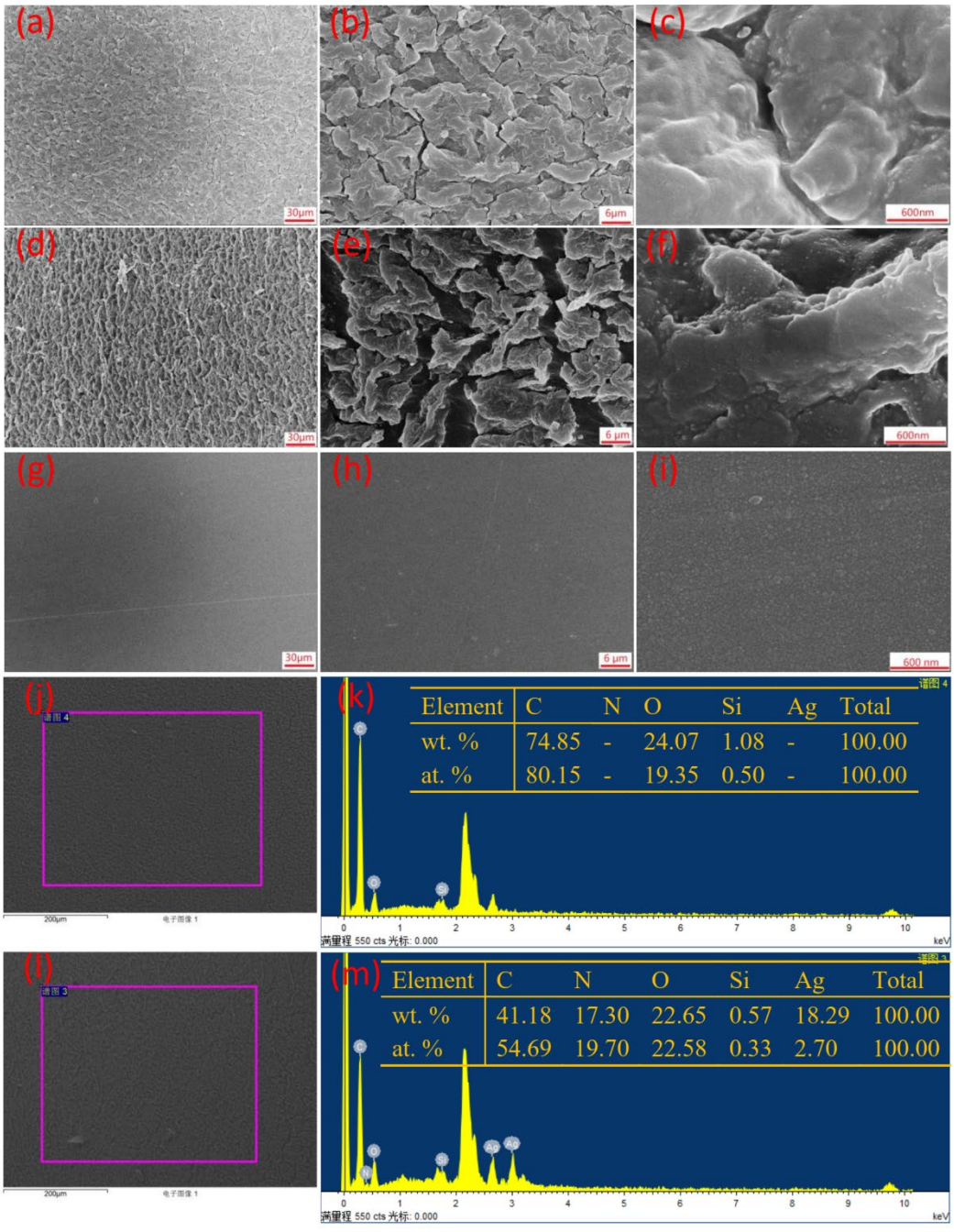

Figure 3 FE-SEM images and EDS analysis of the original urinary catheter, the PDA-CMC-AgNPs coating on the catheter, and the PDA coating on the 304 SS substrate. (a), (b), and (c): the

microtopography of the original urinary catheter magnified with 1,000 X, 5,000 X, and 100,000 X, respectively; (d), (e), and (f): the microtopography of the coated urinary catheter magnified with 1,000 X, 5,000 X, and 100,000 X, respectively; (g), (h), and (i): the microtopography of the PDA coating on the 304 SS substrate magnified with 1,000 X, 5,000 X, and 100,000 X, respectively; (j) and (l): the block diagrams of EDS elemental tests in the analysis area corresponding to Figures 3a and 3d, respectively; (k) and (m): the EDS energy spectra and the coating components corresponding to Figures 3j and 3l, respectively.

XPS Analysis

X-ray photoelectron spectroscopy (XPS) spectra were employed to further prove the composition of the PDA-CMC-AgNPs (0.01 M) coating. XPS survey of the coating in Figure 4a. exhibited the main peaks of C 1s (283.5 eV) and O 1s (530.68 eV), as well as peak of N 1s (398.5 eV) which indicated the N-C bond from PVP [56, 57]. The high-resolution spectrum in Figure 4b exhibited three different peaks with Si 2s (167.0 eV), Si 2p (101.1 eV), and S 2p (152.1 eV) which might come from the original latex urinary catheter layer [58], as shown in Figure S1f. The high-resolution C 1s spectrum of the coating could be fitted to three peaks at 283.3 eV (C1s-1 in Figure 4c, similarly hereinafter), 284.4 eV (C1s-3), and 285.6 eV (C1s-2), which were assigned to C-OR, C-C, and C-O species, respectively [59]. Similarly, the high-resolution O 1s spectrum at 530.7 eV could be fitted to two peaks at 530.3 eV (O1s-1 in Figure 4d, similarly hereinafter) and 531.53 eV (O1s-2), which were assigned to Si-O group and ·OH species, respectively [59]. Furthermore, the peaks of

C-Auger and O-Auger attributed to the X-ray excited auger electron spectroscopy (AES) spectra, which was the inevitable concomitants of the XPS peaks [60].

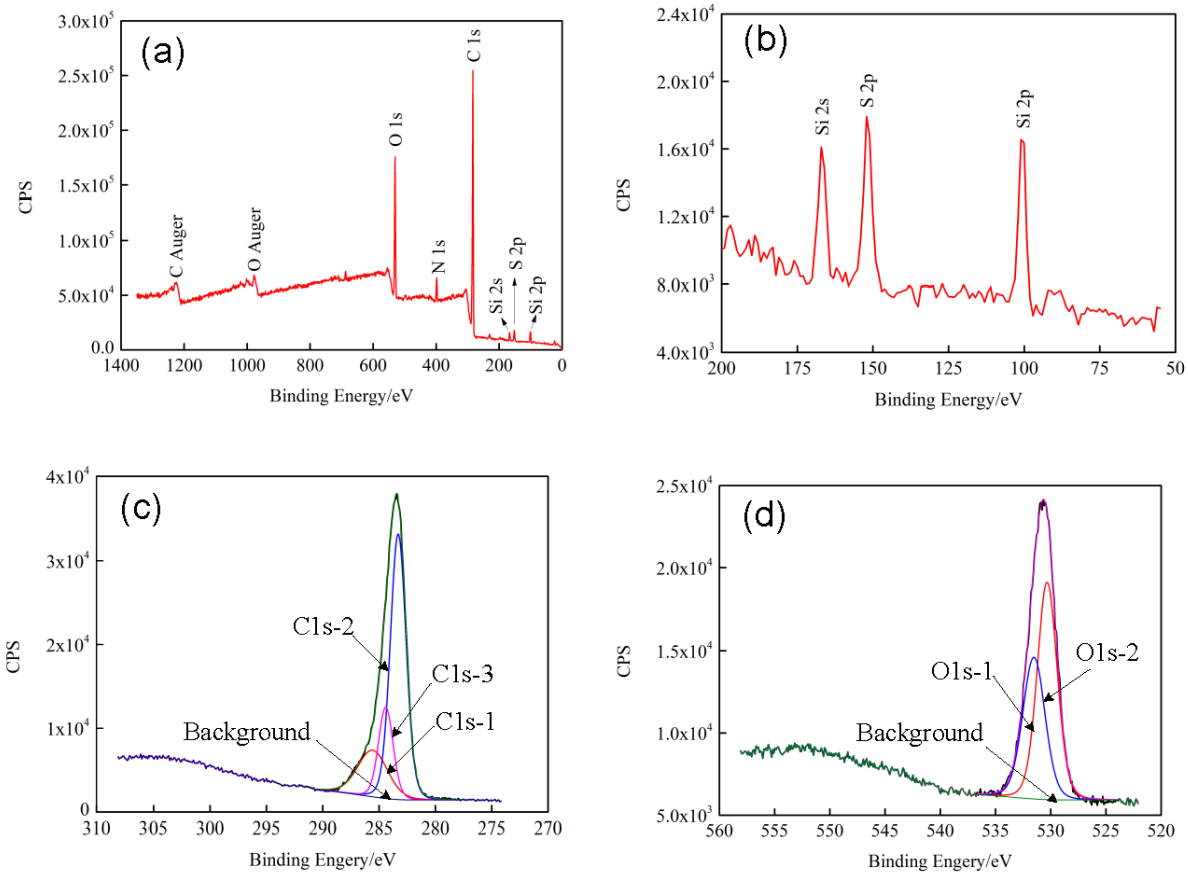

Figure 4 XPS spectra of the PDA-CMC-AgNPs (0.01 M) coated urinary catheter. (a) full-scan spectra; (b), (c), and (d) high-resolution XPS spectra of C 1s, Si 2p, and O 1s.

Contact angle measurement and surface energy calculation

A video optical contact angle measuring instrument was used to measure the contact angle and to determine the wetting properties of the sample surfaces. The contact angle results are shown in

Figure. 5 and Table 1. Figure 5 shows the contact angles measured with the different standard liquids on the uncoated and coated catheters. Clearly the contact angles on the coated catheters were much higher than those on the uncoated catheters. Table 1 further demonstrated that the urinary catheter surface became hydrophobic after coating with the PDA-CMC-AgNPs composites. As a result, the surface free energy, γ_s, of the original urinary catheter was decreased from 30.9 ± 1.7 $mJ \cdot m^{-2}$ to 6.9 ± 1.4 $mJ \cdot m^{-2}$ after the surface coated with the PDA-CMC-AgNPs.

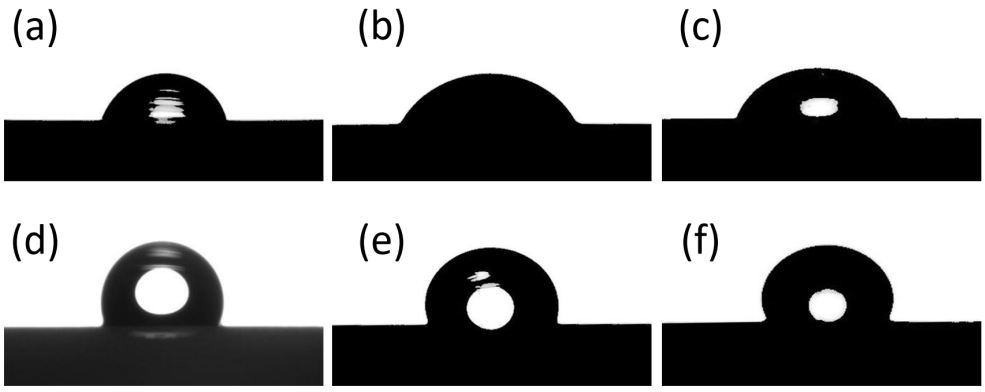

Figure 5 Contact angle measurements (2 μL for each liquid drop); (a), (b), and (c): photographs of the drop shapes of pure water, formamide and diiodomethane on the original catheter, respectively; (d), (e), and (f): photographs of the drop shapes of pure water, formamide, and diiodomethane on the PDA-CMC-AgNPs coated urinary catheter, respectively.

Table 1 Contact angles and surface energies of uncoated and coated catheters.

Sample	Standard liquid	Average angle/°	Surface free energy/$mJ \cdot m^{-2}$
	Water	67.9 ± 1.5	

Original urinary catheter	Formamide	62.8 ± 1.2	30.9 ± 1.7
	Diiodomethane	69.3 ± 3.7	
	Water	114.4 ± 0.9	
PDA-CMC-AgNPs coating	Formamide	104.6 ± 1.1	6.9 ± 1.4
	Diiodomethane	112.4 ± 2.4	

Inhibition zone analysis

The antibacterial activities of the coated catheters were evaluated by examining the inhibition zones against Gram-negative bacteria *E. coli*. The inhibition zones results are summarized in Table 2. The results show the comparisons of inhibition zones of the original uncoated urinary catheter with the coated catheters, including PDA coated catheter, the PDA-CMC-AgNPs coated catheter, and the PDA-CMC-AgNPs coated catheter containing the antibacterial agent CPFX. No inhibition zones were observed around the original uncoated catheter and the PDA-coated catheter segments. Table 2 shows that the inhibition zones of the CMC-AgNPs (0.01 M) coated urinary catheter and the PDA-CMC-AgNPs coated urinary catheter with PDA treatment were all 0.6 cm, indicating that there was no difference against *E. coli* between the two coated catheters. These results demonstrated that the existence of PDA did not improve the antibacterial performance of the coated urinary catheters. However, according to the literature [20], PDA could enhance the adhesion between the coating and the catheter substrate. Table 2 also showed that the inhibition zone of the PDA-CMC-AgNPs coated catheter increased from 0.9 cm to 1.8 cm by adding ciprofloxacin into the PDA-

CMC-AgNPs coating, indicating that ciprofloxacin significantly enhanced the bactericidal property of the coated catheter. However, the addition of antibiotics into catheter coatings was not recommended due to the risk of developing antibiotic-resistant pathogens [10]. Table 2 showed that the increase of the concentration of $AgNO_3$ from 0.01 M to 0.05 M resulted in a slight increase of the diameter of the inhibition zone from 0.8 cm to 1.0 cm. It is well-known that the antibacterial mechanism of Ag nanoparticles is via releasing Ag^+ ions which can interface with the enzymes and sulphydryl groups of proteins, and thus inhibit DNA synthesis of the bacteria [61].

Table 2 Comparison of the inhibition zones against *E. coli* of the coated urinary catheters with those of the original latex urinary catheter.

Samples	Inhibition zone in diameter/cm	Samples	Inhibition zone in diameter/cm
Original urinary catheter	0	CMC-Ag (0.01M)	0.6
PDA	0	PDA-CMC-Ag (0.01M)	0.6
PDA-CMC-Ag (0.01M)	0.8	PDA-CMC-Ag (0.01 M)-CPFX	1.8
PDA-CMC-Ag (0.05M)	1.0	PDA-CMC-Ag	0.9

Live/dead assay: fluorescence microscope images analysis

Figure S2 shows the photographs of the coatings on the SS substrate. The results indicate that the SS substrate showed a mirror color (Figure S2a), and the PDA coating shows a mirror gold color (Figure S2b), while the PDA-CMC-AgNPs shows a lavender color with a slightly uneven color (Figure S2c). Figures 6a-6f show the fluorescence microscopy images impregnated with *S. aureus*

solution after 2 h on the polished SS substrate, the PDA coating, and the PDA-CMC-AgNPs (0.01 M) coating, respectively. Qualitative analysis from Figures 6a and 6b showed that most of bacteria on the original SS sheet were alive. Figures 6c and 6d illustrated that there were large numbers of live and dead bacteria on the PDA coated surface. On the contrary, there were almost no live bacteria on the PDA-CMC-AgNPs (0.01 M) coated stainless steel sheet (Figure 6e), and there were only few dead bacteria on the coated surface(Figure 6f). In other words, the total number of live and dead bacteria on the PDA-CMC-AgNPs (0.01 M) coating was much less than those on the PDA coating and on the SS substrate, which indicated that the PDA-CMC-AgNPs (0.01 M) coating not only had a good antibacterial effect, but also had a good non-stick property to bacteria.

The number of adhered bacteria was counted by Image-ProPlus® and the result was given in Figure 6g. Compared to the SS substrate, the quantitative analysis from Figure 6g indicated that the numbers of live and dead bacteria on the PDA coating were reduced by 20.9% and 10.7%, respectively, compared with the uncoated surface. While, the numbers of live and dead bacteria on the PDA-CMC-AgNPs (0.01 M) coating were reduced by 99.0% and 86.6%, respectively, compared with the uncoated surface which demonstrated the strong anti-bacterial and anti-adhesion properties of the PDA-CMC-AgNPs (0.01 M) coating. The non-stick property of the PDA-CMC-AgNPs (0.01 M) coating might attribute to the low surface energy (Table 1).[62]

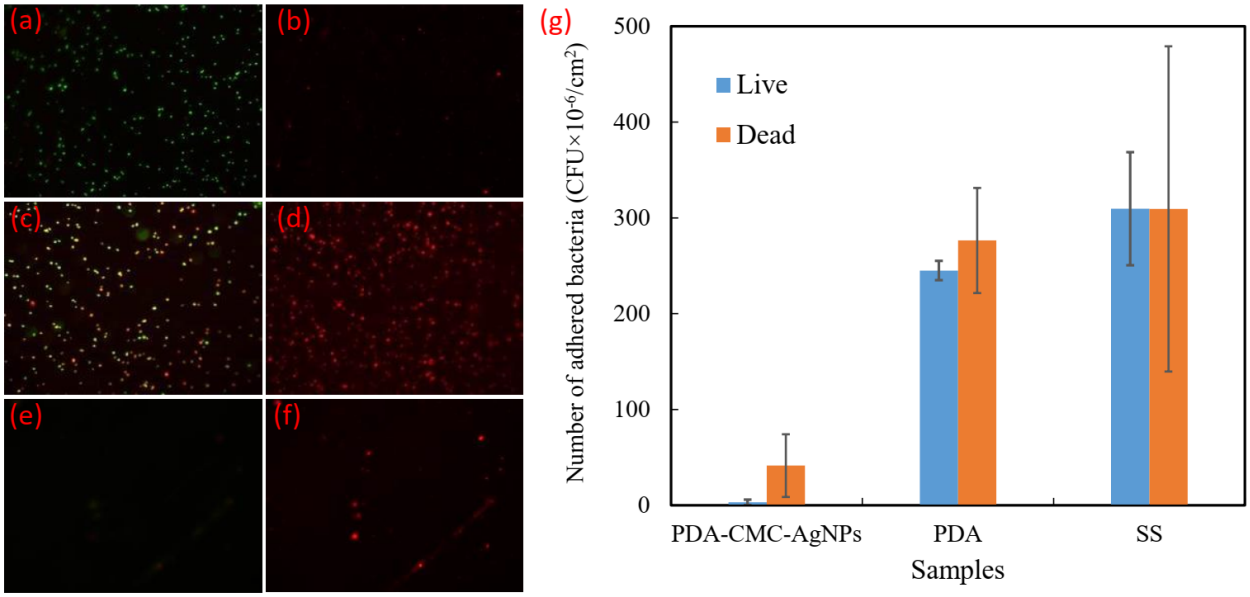

Figure 6 The fluorescence microscopy images impregnated with *S. aureus* solution after 2 h; (a) and (b): living bacteria (green) and dead bacteria (red) on the original SS sheet, respectively; (c) and (d): living bacteria (green) and dead bacteria (red) on the PDA coating, respectively; (e) and (f): live bacteria (green) and dead bacteria(red) on the PDA-CMC-AgNPs (0.01 M) coating, respectively; (g): comparison of adherence of dead and live *S. aureus* bacteria on different samples.

Conclusion

The polydopamine-carboxymethylcellulose-AgNPs (PDA-CMC-AgNPs) coatings with antibacterial and anti-adhesion properties to bacteria were prepared on the Foley urinary catheters. The color of the catheters coated with polydopamine and carboxymethyl cellulose became darker and the bond strength between the coating and the urinary catheter surface was strong. TEM revealed the well-dispersed quasi-spherical-shaped silver nano-particles with the average diameter of 24.5 ±

4.1 nm. The PDA-CMC-AgNPs (0.01 M) coating revealed a smoother surface compared with the original catheter, which might contribute to the super-lubricity property of the coated catheter. The contact angle of the coated catheter was larger than that of the original uncoated catheter. The surface free energy of the original uncoated catheter was reduced from 30.9 ± 1.7 $mJ \cdot m^{-2}$ to 6.9 ± 1.4 $mJ \cdot m^{-2}$ after being coated with the PDA-CMC-AgNPs.

The inhibition zone analysis showed that both the original uncoated catheter and the PDA-coated catheter had no antibacterial effect, and the addition of PDA did not improve the antibacterial performance of the CMC hydrogel coating. The bactericidal performance of the CMC-AgNPs coated catheter was significantly enhanced by adding ciprofloxacin to the CMC-AgNPs hydrogel. The increase of the concentration of $AgNO_3$ resulted in the enhancement of the antibacterial properties of the coated urinary catheter. The PDA-CMC-AgNPs (0.01 M) coating inhibited 99.0% of live bacteria and decreased the adhesion to dead bacteria by 86.6%. The anti-adhesion property of the PDA-CMC-AgNPs (0.01 M) coating attributed to the low surface energy of the coating.

Acknowledgments

Research for this paper was partially supported by Natural Science Foundation of Chongqing Municipality (No. cstc2020jcyj-msxmX0579), UK Engineering and Physical Sciences Research Council (No. EP/P00301X/1), Special Project of Science and Technology Talent of Banan District Science and Technology Bureau of Chongqing Municipality (No. 2020TJZ015), Project of Chongqing Municipality Innovative Talent Training Project for Primary and Secondary Schools (No.

CY200903), and Special Project of Research Development of Banan District of Chongqing Municipality (No. 2020QC383).

Authorship contributions

Yongwei Cai: Conceptualization, Methodology, Resources, Figure polishing, Writing original draft, Project administration. **Ronghua Gu**: Investigation, Formal analysis, Antibacterial performance tests, Writing original draft. **Yuhang Dong:** Investigation, Manuscript revision and language polishing. **Qi Zhao**: Conceptualization, Resources, Manuscript revision and language polishing, Supervision, Project administration. **Ke Zhang**: Investigation, Inhibition zone analysis. **Changyuan Cheng**: Investigation, Fluorescence Microscope images analysis. **Hong Yang**: FE-SEM analysis, Contact angle measurement. **Jianxiang Li**: XPS analysis. **Xing'gen Yuan**: Surface energy calculation.

Authors information

Corresponding authors:

Yongwei Cai − Department of Chemistry and Chemical Engineering, Chongqing University of Technology, Chongqing 400054, China; orcid.org/0000-0002-7705-3077; Phone: +86 23 6256 3617; Fax: +86 23 6256 3221; Email: cyw@cqut.edu.cn

Qi Zhao – School of Science & Engineering, University of Dundee, Dundee DD1 4HN, U.K.; orcid.org/0000-0002-4831-1727; Phone: +44 1382 385651; Fax: +44 1382 385508; Email: q.zhao@dundee.ac.uk

Compliance with ethical standards

Conflict of interest: We declare that we have no financial and personal relationships with other people or organizations that can inappropriately influence our work.

Supplementary information: Supplementary data associated with this article can be found in the online version.

References

1. Siddiq DM, Darouiche RO. New strategies to prevent catheter-associated urinary tract infections. *Nat Rev Urol* 2012; 9: 305-314.

2. Zhu Z, Wang Z, Li S, et al. Antimicrobial strategies for urinary catheters. *J Biomed Mater Res A* 2019; 107: 445-467.

3. Zhang S, Wang L, Liang X et al. Enhanced antibacterial and antiadhesive activities of silver-PTFE nanocomposite coating for urinary catheters. *ACS Biomater Sci Eng* 2019; 5: 2804-2814.

4. Flores-Mireles AL, Walker JN, Caparon M, et al. Urinary tract infections: epidemiology, mechanisms of infection and treatment options. *Nat Rev Microbiol* 2015; 13: 269-284.

5. Islas L, Alvarez-Lorenzo C, Magarinos B, et al. Singly and binary grafted poly (vinyl chloride) urinary catheters that elute ciprofloxacin and prevent bacteria adhesion. *Int J Pharmaceut* 2015; 488: 20-28.

6. Aljohi AA, Hassan HE, Gupta RK. The efficacy of noble metal alloy urinary catheters in reducing catheter-associated urinary tract infection. *Urol Ann* 2016; 8: 423-429.

7. Jing Y, Mu B, Zhang M, et al. Zinc-loaded palygorskite nanocomposites for catheter coating with excellent antibacterial and anti-biofilm properties. *Colloids Surf A* 2020; 600: 124965.

8. Lawrence EL, Turner IG. Materials for urinary catheters: a review of their history and development in the UK. *Med*

Eng Phys 2005; 27: 443-453.

9. Shen J, Chen R, Wang J, et al. One-step surface modification strategy with composition-tunable microgels: From bactericidal surface to cell-friendly surface. *Colloids Surf B* 2022; 212: 112372.

10. Keum H, Kim JY, Yu B, et al. Prevention of bacterial colonization on catheters by a one-step coating process involving an antibiofouling polymer in water. *ACS Appl Mater Interfaces* 2017; 9: 19736-19745.

11. Kamal GD, Pfaller MA, Rempe LE, et al. Reduced intravascular catheter infection by antibiotic bonding: a prospective, randomized, controlled trial. *Jama* 1991; 265: 2364-2368.

12. Divya M, Kiran GS, Hassan S, et al. Biogenic synthesis and effect of silver nanoparticles (AgNPs) to combat catheter-related urinary tract infections. *Biocatal Agric Biotechnol* 2019; 18: 101037.

13. Zhang S, Liang X, Gadd GM et al. A sol–gel based silver nanoparticle/polytetrafluorethylene (AgNP/PTFE) coating with enhanced antibacterial and anti-corrosive properties. *Appl Surf Sci* 2021; 535: 147675.

14. Wang B, Quan Y, Xu Z, et al. Preparation of highly effective antibacterial coating with polydopamine/chitosan/silver nanoparticles via simple immersion. *Prog Org Coat* 2020; 149: 105967.

15. Meeker DG, Jenkins SV, Miller EK, et al. Synergistic photothermal and antibiotic killing of biofilm-associated Staphylococcus aureus using targeted antibiotic-loaded gold nanoconstructs. *ACS Infect Dis* 2016; 2: 241-250.

16. Kalaivani S, Singh RK, Ganesan V, et al. Effect of copper (Cu^{2+}) inclusion on the bioactivity and antibacterial behavior of calcium silicate coatings on titanium metal. *J Mater Chem B* 2014; 2: 846-858.

17. Panaček A, Kvitek L, Prucek R, et al. Silver colloid nanoparticles: synthesis, characterization, and their antibacterial activity. *J Phys Chem B* 2006; 110: 16248-16253.

18. Dakal TC, Kumar A, Majumdar RS, et al. Mechanistic basis of antimicrobial actions of silver nanoparticles. *Front*

Microbiol 2016; 7: 1831.

19. Singha P, Locklin J, Handa H. A review of the recent advances in antimicrobial coatings for urinary catheters, *Acta Biomater* 2017; 50: 20-40.

20. Lee H, Dellatore SM, Miller WM, et al. Mussel-inspired surface chemistry for multifunctional coatings. *Science* 2007; 318: 426-430.

21. Li Y, Li C, Yu R, et al. Application of polydopamine on the implant surface modification. *Polym Bull* 2022; 79: 5613-5633.

22. Wang Y, Huang Q, He X, et al. Multifunctional melanin-like nanoparticles for bone-targeted chemo-photothermal therapy of malignant bone tumors and osteolysis. *Biomaterials* 2018; 183: 10-19.

23. Lynge ME, Ogaki R, Laursen AO, et al. Polydopamine/liposome coatings and their interaction with myoblast cells. *ACS Appl. Mater. Interfaces* 2011; 3: 2142-2147.

24. Tsai WB, Chen WT, Chien HW, et al. Poly (dopamine) coating of scaffolds for articular cartilage tissue engineering. *Acta Biomater* 2011; 7: 4187-4194.

25. Chen D, Zhao L, Hu W. Protein immobilization and fluorescence quenching on polydopamine thin films. *J Colloid Interface Sci* 2016; 477: 123-130.

26. Postma A, Yan Y, Wang Y, et al. Self-polymerization of dopamine as a versatile and robust technique to prepare polymer capsules. *Chem Mater* 2009; 21: 3042-3044.

27. Yeroslavsky G, Richman M, Dawidowicz L, et al. Sonochemically produced polydopamine nanocapsules with selective antimicrobial activity. *Chem Commun* 2013; 49: 5721-5723.

28. Ling D, Park W, Park YI, et al. Multiple‐interaction ligands inspired by mussel adhesive protein: synthesis of

highly stable and biocompatible nanoparticles. *Angew Chem Int Ed* 2011; 50: 11360-11365.

29. McCloskey BD, Park HB, Ju H, et al. Influence of polydopamine deposition conditions on pure water flux and foulant adhesion resistance of reverse osmosis, ultrafiltration, and microfiltration membranes. *Polymer* 2010; 51: 3472-3485.

30. Huang L, Yi J, Gao Q, et al. Carboxymethyl chitosan functionalization of CPED-treated magnesium alloy via polydopamine as intermediate layer. *Surf Coat Technol* 2014; 258: 664-671.

31. Xu J, Xu N, Zhou T, et al. Polydopamine coatings embedded with silver nanoparticles on nanostructured titania for long-lasting antibacterial effect. *Surf Coat Technol* 2017; 320: 608-613.

32. Ku SH, Ryu J, Hong SK, et al. General functionalization route for cell adhesion on non-wetting surfaces. *Biomaterials* 2010; 31: 2535-2541.

33. Liu Y, Ai K, Liu J, et al. Dopamine‐melanin colloidal nanospheres: an efficient near‐infrared photothermal therapeutic agent for in vivo cancer therapy. *Adv Mater* 2013; 25: 1353-1359.

34. Zhong S, Luo R, Wang X, et al. Effects of polydopamine functionalized titanium dioxide nanotubes on endothelial cell and smooth muscle cell. *Colloids Surf B* 2014; 116: 553-560.

35. Fan H, Gong JP. Fabrication of bioinspired hydrogels: challenges and opportunities. *Macromolecules* 2020; 53: 2769-2782.

36. Yong Y, Qiao M, Chiu A, et al. Conformal hydrogel coatings on catheters to reduce biofouling. *Langmuir* 2018; 35: 1927-1934.

37. Chen Z, Mo M, Fu F, et al. Antibacterial structural color hydrogels. *ACS Appl Mater Interfaces* 2017; 9: 38901-38907.

38. Li S, Dong S, Xu W, et al. Antibacterial hydrogels. *Adv Sci* 2018; 5: 1700527.

39. Han W, Zhou B, Yang K, et al. Biofilm-inspired adhesive and antibacterial hydrogel with tough tissue integration performance for sealing hemostasis and wound healing. *Bioact Mater* 2020; 5: 768-778.

40. Wang L, Zhang X, Yang K, et al. A novel double-crosslinking-double-network design for injectable hydrogels with enhanced tissue adhesion and antibacterial capability for wound treatment. *Adv Funct Mater* 2020; 30: 1904156.

41. Buwalda SJ, Boere KW, Dijkstra PJ, et al. Hydrogels in a historical perspective: From simple networks to smart materials. *J Controlled Release* 2014; 190: 254-273.

42. Hamidi M, Azadi A, Rafiei P. Hydrogel nanoparticles in drug delivery. *Adv Drug Delivery Rev* 2008; 60: 1638-1649.

43. Rudy A, Kuliasha C, Uruena J, et al. Lubricous hydrogel surface coatings on polydimethylsiloxane (PDMS). *Tribol Lett* 2017; 65: 1-11.

44. Cong HP, Wang P, Yu SH, et al. Highly elastic and superstretchable graphene oxide/polyacrylamide hydrogels. *Small* 2014; 10: 448-453.

45. Huang X, Ge M, Wang H, et al. Functional modification of polydimethylsiloxane nanocomposite with silver nanoparticles-based montmorillonite for antibacterial applications. *Colloids Surf A* 2022; 642: 128666.

46. Ghorpade VS, Yadav AV, Dias RJ, et al. Citric acid crosslinked carboxymethylcellulose-poly (ethylene glycol) hydrogel films for delivery of poorly soluble drugs. *Int J Biol Macromol* 2018; 118: 783-791.

47. Yadollahi M, Namazi H, Aghazadeh M, et al. Antibacterial carboxymethyl cellulose/Ag nanocomposite hydrogels cross-linked with layered double hydroxides. *Int J Biol Macromol* 2015; 79: 269-277.

48. Aradmehr A, Javanbakht V. A novel biofilm based on lignocellulosic compounds and chitosan modified with silver

nanoparticles with multifunctional properties: Synthesis and characterization. *Colloids Surf A* 2020; 600: 124952.

49. Roto R, Rasydta HP, Suratman A, et al. Effect of reducing agents on physical and chemical properties of silver nanoparticles. *Indones J Chem* 2018; 18: 614-620.

50. Saha N, A. Saarai A, Roy R, et al. Polymeric biomaterial based hydrogels for biomedical applications. *J Biomater Nanobiotechnol* 2011; 2: 85-90.

51. Cai Y, Liu M. Corrosion behavior of titania films coated by liquid-phase deposition on AISI304 stainless steel substrates. *AIChE J* 2012; 58: 1907-1920.

52. Michalski M, Hardy J, Saramago BJ, et al. On the surface free energy of PVC/EVA polymer blends: comparison of different calculation methods. *J Colloid Interface Sci* 1998; 208: 319-328.

53. Ryan KJ, Schoenknecht FD, Kirby WMM, et al. Disc sensitivity testing. *Hosp Pract* 1970; 5: 91-100.

54. Nersisyan HH, Lee JH, Son HT, et al. A new and effective chemical reduction method for preparation of nanosized silver powder and colloid dispersion. *Mater Res Bull* 2003; 38: 949-956.

55. Boussu K, Van der Bruggen B, Volodin A, et al. Roughness and hydrophobicity studies of nanofiltration membranes using different modes of AFM. *J Colloid Interface Sci* 2005; 286: 632-638.

56. Zhu J, Tang T, Hu C, et al. Cellulose nanocrystal assisted trace silver nitrate to synthesize green silver nanocomposites with antibacterial activity. *RSC Adv* 2021; 11: 3808-3815.

57. Chang X, Wang Z, Quan S, et al. Exploring the synergetic effects of graphene oxide (GO) and polyvinylpyrrodione (PVP) on poly (vinylylidenefluoride) (PVDF) ultrafiltration membrane performance. *Appl Surf Sci* 2014; 316: 537-548.

58. Yu H, Liu L, Li X, et al. Fabrication of polylysine based antibacterial coating for catheters by facile electrostatic

interaction. *Chem Eng J* 2019; 360: 1030-1041.

59. Crist BV. Handbook of monochromatic XPS spectra: The elements of native oxides. *John Wiley & Sons*, 2000.

60. Cai Y, Li S, Cheng ZG, et al. Facile fabrication of super-hydrophobic FAS modified electroless Ni-P coating meshes for rapid water-oil separation. *Colloids Surf A* 2018, 540: 224-232.

61. Divya M, Kiran GS, Hassan S, et al. Biogenic synthesis and effect of silver nanoparticles (AgNPs) to combat catheter-related urinary tract infections. *Biocatal Agric Biotechnol* 2019; 18: 101037.

62. Li J, Wang G, Meng Q, et al. A biomimetic nano hybrid coating based on the lotus effect and its anti-biofouling behaviors. *Appl Surf Sci* 2014; 315: 407-414.